Preparation of $H_3PMo_{12}O_{40}$/organobentonite by chemical immobilization method and its catalytic performance in photo-Fenton process

Lin-Ye Zhang[a,b], Shu-Ya Cai[a], Kai Huang[a,c], Zhong-Min Li[a], Guang-Tao Wei[a,d,*], Xuan-Hai Li[a], Ji-Hua Mo[b], You-Chang Liang[a]

[a]*School of Chemistry and Chemical Engineering, Guangxi University, Nanning Guangxi 530004, China*
Tel. +86 771 323 3718; email: gtwei@gxu.edu.cn
[b]*Ministry-Province Jointly-Constructed Cultivation Base for State Key Laboratory of Processing for Non-Ferrous Metal and Featured materials, Nanning Guangxi 530004, China*
[c]*Guangxi Key Laboratory of Biorefinery, Guangxi Academy of Sciences, Nanning Guangxi 530007, China*
[d]*Key Laboratory of New Processing Technology for Nonferrous Metals and Materials, Ministry of Education, Guangxi University, Nanning Guangxi 530004, China*

ABSTRACT

Homogeneous photo-Fenton process has some significant disadvantages in wastewater treatment. Heterogeneous photo-Fenton process overcomes the disadvantages of homogeneous photo-Fenton process, and shows good prospects in engineering application. In this study, $H_3PMo_{12}O_{40}$/organobentonite was prepared by a chemical immobilization method, and catalytic performance of $H_3PMo_{12}O_{40}$/organobentonite as heterogeneous catalyst in photo-Fenton process was evaluated by adopting methyl orange (MO) dye as a model pollutant. The removal ratio of MO was impacted by reaction time, H_2O_2 concentration, and initial MO concentration. $H_3PMo_{12}O_{40}$/organobentonite had a wide applicable range of pH and temperature for wastewater treatment. $H_3PMo_{12}O_{40}$/organobentonite had a long-term stability, and retained almost all of its catalytic stability and activity for four recycling times. Characterization results of $H_3PMo_{12}O_{40}$/organobentonite showed that $H_3PMo_{12}O_{40}$ was successfully immobilized on the organobentonite by the chemical immobilization method. The possible mechanisms involving in both catalyst preparation and photo-Fenton process were presented in this paper. $H_3PMo_{12}O_{40}$/organobentonite was successfully prepared by the chemical immobilization method through grafting. $H_3PMo_{12}O_{40}$/organobentonite as heterogeneous catalyst had certain advantages for practical use in photo-Fenton process.

Keywords: Heteropoly acid; Phosphomolybdic acid; Chemical immobilization method; Bentonite; Photo-Fenton; Methyl orange

1. Introduction

Photo-Fenton as one advanced oxidant process has been proven to be a promising technology for wastewater treatment [1,2]. However, homogeneous photo-Fenton process has some significant disadvantages including narrow applicable range of pH, difficult separation of catalyst, and no reuse for catalyst. Based on the advantages of heterogeneous catalyst, heterogeneous photo-Fenton process, i.e.

*Corresponding author.

photo-Fenton catalyzed by heterogeneous catalyst, overcomes these disadvantages of homogeneous photo-Fenton process. Therefore, much attention has been focused on development of heterogeneous catalyst used in photo-Fenton process [3–5]. With these heterogeneous catalysts, heterogeneous photo-Fenton process showed good prospects in engineering application.

Heteropolyacid (HPA) is a multi-function catalyst among the most promising catalysts because of its special catalytic action and wonderful application foreground [6], and photo-catalysis catalyzed by HPA is a new branch in the field of photo-catalytic chemistry [7]. Recently, some attractive progress in the HPA-catalysed photo-Fenton process has been made [8–10]. Nevertheless, the low specific surface area ($<10\,m^2/g$) of HPA catalysts limits its efficacy. This problem has been partly solved by impregnation of HPAs on inorganic mesoporous materials, such as mesoporous molecular sieves (MCM-41, HMS), mesoporous silicas (SBA-15), carbon gels, and γ-aluminaby [11]. However, due to the high solubility of HPAs in polar solvents, HPAs physically adsorbed on the surface of the support can be easily leached out [12,13]. Chemical immobilization has been attempted to immobilize HPAs onto the surface of mesoporous materials by grafting, that is, by providing an anchoring site for heteropolyanion. If the supporting material is modified to have a positive charge by grafting, the HPA molecule can be chemically and molecularly immobilized on the supporting material. Mesostructured cellular foam silica was functionalized with 3-aminopropyltriethoxysilane ($H_2N(CH_2)_3Si(OC_2H_5)_3$, APTES), whereby the surface hydroxyl group of the support reacted with a ethoxysilane group and HPAs with theterminal amine group ($-NH_2$) of APTES [11,14]. The surface of acid-activated palygorskite (Pa) was modified by grafting APTES (the product denoted as Pa_{APTES}) for immobilization of phosphotungstic acid ($H_3PW_{12}O_{40}$, HPW), and the prepared HPW/Pa_{APTES} provided a satisfactory option for catalyzing esterification reaction [15].

Bentonite, a form of natural and impure clay, consists of a primary mineral called montmorillonite. Montmorillonite is a layered, dual-dimensional mineral that has aluminum and silicate, and the crystals of montmorillonite consist of three layers: a silicon tetrahedron, an aluminum octahedron, and another silicon tetrahedron. The unit structure of montmorillonite is a very thin platelet. Bentonite has particular properties and structures as well as abundance in world and low cost, so it had been used to prepare clay-based heterogeneous catalyst which was used in photo-Fenton systems. Many research results showed

that the clay-based heterogeneous catalysts were catalytically more effective and more resistant to leaching than other Fenton-like catalysts [4,16–19].

In this work, we prepared $H_3PMo_{12}O_{40}$/organobentonite by a chemical immobilization method, which was a novel heterogeneous catalyst used in photo-Fenton process. Moreover, due to the environmental significance and non-biodegradation of methyl orange (MO) dye, catalytic performance of $H_3PMo_{12}O_{40}$/organobentonite as heterogeneous catalyst in photo-Fenton process was evaluated by adopting MO dye as a model pollutant.

2. Experimental

2.1. Materials and reagents

Bentonite was purchased from Shanghai No. 4 Reagent and H.V. Chemical Limited Company; MO, H_2O_2 (30%), cetyltrimethylammonium bromide (CTAB), H_2SO_4, NaOH, and $H_3PMo_{12}O_{40}$ were purchased from Shanghai Chemical Reagent Company. All reagents were of analytical grade and used without further purification. The structure and characteristics of MO were given in Table 1.

2.2. Catalyst preparation

Organobentonite was prepared as follows: CTAB was added slowly as a powder into the aqueous dispersion of bentonite (5%) under stirring. The dispersion was stirred for 2 h under 80°C, and then the insoluble material was filtered, followed by rinsing with deionized water until Br^- was undetectable by $AgNO_3$. The prepared organobentonite was dried at 80°C and ground to less than 0.15 mm.

$H_3PMo_{12}O_{40}$/organobentonite was prepared as follows: $H_3PMo_{12}O_{40}$ was added slowly as a powder

Table 1
Properties of MO

Index	Methyl orange
Molecular structure	NaO$_2$S—⬡—N=N—⬡—N(CH$_3$)$_2$
Molecular formula	$C_{14}H_{14}N_3NaO_3S$
Molecular weight	327.33
Hazard class	6.1
Hazard codes	*T*
Safety statements	45–24/25–16–36/37/39
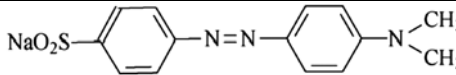
into the aqueous dispersion of organobentonite (13%) under stirring, until the mass ratio of [$H_3PMo_{12}O_{40}$]/ [organobentonite] became 0.02:1. After the mixture was stirred for 3.5 h, the insoluble material was filtered. The solid product was dried at 105°C and then was calcined at 200°C for 1.5 h. The prepared $H_3PMo_{12}O_{40}$/organobentonite catalyst was then ground to less than 0.15 mm.

2.3. Catalytic experiment setup and reaction solution analysis

The photo-Fenton degradation of 400 mL MO solution was carried out in a 500 mL glass cylindrical reactor (20 cm inner length, 10 cm inner diameter), which was placed inside a 600 mm × 550 mm × 450 mm stainless steel box with a door in one side for operating. The UV irradiation source was a UV light tube (40 W, 365 nm) positioned on the roof of stainless steel box, and the distance between the UV light tube and the reaction mixture was about 400 mm. The reaction mixture was stirred magnetically during irradiation. The initial pH value of the solution was adjusted by adding NaOH or H_2SO_4. The solution samples were taken at desired time intervals, and then centrifuged to separate catalyst from the suspension. The remaining MO in sample solution was determined using UV-visible Spectrophotometer (UV-1,201, BFRL, China) at 464 nm which is the maximum absorbance wavelength of the MO solution. All experiments for testing were run three times and the averages were taken to eradicate any discrepancies. Prior to measurement, a calibration curve was plotted. The catalytic performance of $H_3PMo_{12}O_{40}$/organobentonite in photo-Fenton process was evaluated by the removal ratio of MO which was calculated with the following formula:

$$\eta = \left(1 - \frac{C_t}{C_0}\right) \times 100\% \tag{1}$$

where C_t and C_0 represent the time-dependent concentration and the initial concentration, respectively.

2.4. Catalyst characterization

The X-ray diffraction (XRD) patterns of the catalyst were measured with a Rigaku D/MAX-IIIA X-ray diffractometer equipped with Cu Ka radiation. The FT-IR spectra of the catalyst were recorded by the KBr pellet technique on a NEXUS-470 Fourier-transform infrared spectrometer. The scanning electron microscopy (SEM) pictures of the catalyst were recorded on a HITACHI S-3000 N scanning electron microscope.

3. Results and discussion

3.1. Concentration of CTAB to bentonite used in organobentonite for catalyst preparation

Organobentonite was prepared with different CTAB concentration to bentonite (n_{CTAB}/m_{Bent}), and the n_{CTAB}/m_{Bent} effect on the adsorption ability of organobentonite was shown in Fig. 1. Increase in n_{CTAB}/m_{Bent} increased the adsorption of MO. The removal ratio of MO increased to 86.1% from 3.04% in the n_{CTAB}/m_{Bent} range from 0.08 to 0.50 mmol/g. High CTAB content organobentonite has excellent adsorption ability for organic pollutants in wastewater [20,21]. In order to study $H_3PMo_{12}O_{40}$/organobentonite catalytic performance as heterogeneous catalyst in photo-Fenton system, organobentonite with little MO adsorption ability should be chosen to prepare $H_3PMo_{12}O_{40}$/organobentonite. The removal ratio of MO only reached 9.0% for organobentonite of n_{CTAB}/m_{Bent} 0.17 mmol/g; so, organobentonite of n_{CTAB}/m_{Bent} 0.17 mmol/g was used to prepare $H_3PMo_{12}O_{40}$/organobentonite for further experiments.

3.2. Effect of catalyst dosage on the adsorption of MO

As shown in Fig. 2, increase in the $H_3PMo_{12}O_{40}$/organobentonite dosage increased the adsorption of MO. However, the removal ratio of MO only reached 9.0% at $H_3PMo_{12}O_{40}$/organobentonite dosage 1.0 g/L. In order to study $H_3PMo_{12}O_{40}$/organobentonite catalytic performance as heterogeneous catalyst in
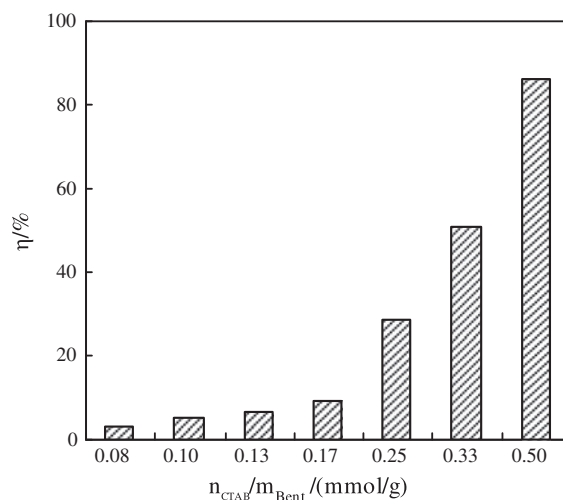
Fig. 1. Effect of n_{CTAB}/m_{Bent} on the adsorption ability of organobentonite. Data in figure are average of experimental data. The experimental conditions were conducted under conditions: [organobentonite] = 1 g L^{-1}, [MO] = 10 mg L^{-1}, t = 60 min, T = 30°C and initial pH of solution.
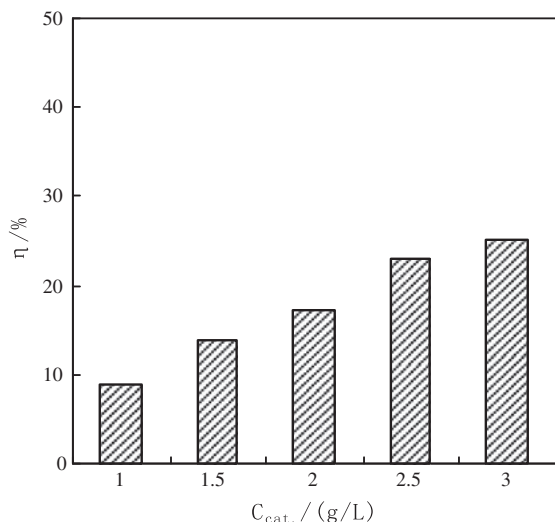
Fig. 2. Effect of catalyst dosage on the adsorption of MO. Data in figure are average of experimental data. The experimental conditions were conducted under conditions: $[MO] = 10 \, mg \, L^{-1}$, $t = 60 \, min$, $T = 30 \, ^\circ C$ and initial pH of solution.

Fig. 3a. Effect of reaction time and H_2O_2 concentration ($\blacklozenge$ 2.2 mmol L^{-1}, $\square$ 4.4 mmol L^{-1}, $\blacktriangle$ 8.8 mmol L^{-1}, $\diamondsuit$ 17.6 mmol L^{-1}) on the removal ratio of MO. The experimental conditions were conducted under conditions: $[MO] = 10 \, mg \, L^{-1}$, $[H_3PMo_{12}O_{40}/organobentonite] = 1 \, g \, L^{-1}$, $T = 30 \, ^\circ C$, initial pH of solution.

photo-Fenton system, a dosage of $H_3PMo_{12}O_{40}/$ organobentonite with little MO adsorption ability should be chosen in photo-Fenton degradation experiments. Hence, a $H_3PMo_{12}O_{40}/organobentonite$ dosage of 1.0 g/L was used as the catalyst dosage in the photo-Fenton degradation of MO for further experiments.

3.3. Catalytic performance of $H_3PMo_{12}O_{40}/organobentonite$ in photo-Fenton process

At the $H_3PMo_{12}O_{40}/organobentonite$ dosage 1.0 g/L, the effect of reaction time and H_2O_2 concentration on the removal ratio of MO was investigated. As shown in Fig. 3(a), increase in the reaction time increased the degradation of MO. However, it should be pointed out that when the reaction time was over 120 min with the H_2O_2 concentration of 4.4, 8.8, and 17.6 mmol/L, the removal ratio of MO increased slightly which indicated that degradation balance of MO was reached at reaction time of 120 min. Increase in the H_2O_2 concentration from 2.2 to 17.6 mmol/L increased the degradation of MO. The acceleration of degradation of MO by addition of H_2O_2 was due to increase in hydroxyl radicals, which increased the probability of attack of MO molecules by hydroxyl radicals. However, there was no significant improvement in removal ratio of MO when the H_2O_2 dosage exceeded 8.8 mmol/L. For example, compared with the removal ratio of MO 87.9% at 120 min with the H_2O_2 concentration of 8.8 mmol/L, the removal ratio only reached 91.3% at 120 min with the H_2O_2

concentration of 17.6 mmol/L. This was due to the fact that at a higher H_2O_2 concentration, scavenging of hydroxyl radicals occurred, which led to decrease in the number of hydroxyl radicals in solution through Eqs. (2) and (3) [22,23]. Hence, a H_2O_2 dosage of 8.8 mmol/L was used as the optimum dosage in the degradation of MO for further experiments.

$$H_2O_2 + \cdot OH \rightarrow H_2O + \cdot HO_2 \qquad (2)$$

$$\cdot HO_2 + \cdot OH \rightarrow H_2O + O_2 \qquad (3)$$

The results of initial pH of solution on removal ratio of MO were shown in Fig. 3(b). Our findings was significantly different from the previous reports [24,25], and it was interesting to note that the removal ratio of MO kept a relatively high percentage even at high pH. The removal ratio of MO was 90.7% at pH 3, while the removal ratio of MO only decreased to 85.0% at pH 9. The solution pH of homogeneous photo-Fenton process should be adjusted to near 3 to reach high degradation efficiency in wastewater treatment. Moreover, in homogeneous photo-Fenton process, the catalyst of metal ions produces hydroxide sludge in high pH range, which usually makes the metal ions lost their catalytic performance. Compared with the pH controlled at around 3 in using for homogeneous photo-Fenton process, $H_3PMo_{12}O_{40}/$ organobentonite used as heterogeneous catalyst in photo-Fenton process had a wider applicable range of pH, and $H_3PMo_{12}O_{40}/organobentonite$ kept high

(b)
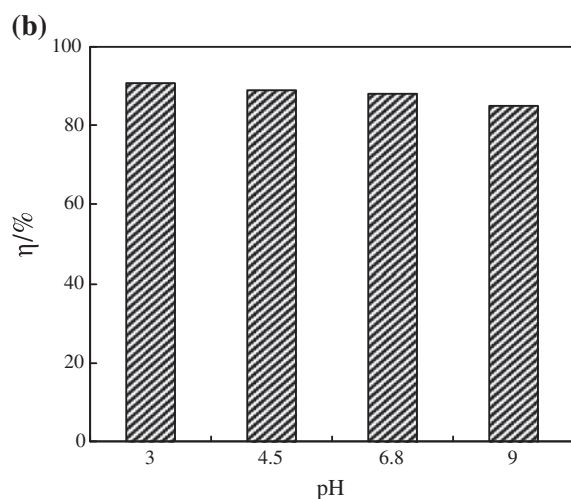
Fig. 3b. Initial pH of solution on removal ratio of MO. The experimental conditions were conducted under conditions: $[MO] = 10 \, mg \, L^{-1}$, $[H_2O_2] = 8.8 \, mmol \, L^{-1}$, $t = 120 \, min$, $[H_3PMo_{12}O_{40}/organobentonite] = 1 \, g \, L^{-1}$, $T = 30 \, ℃$.

catalytic performance at high pH. Therefore, $H_3PMo_{12}O_{40}$/organobentonite had certain advantages for practical application in photo-Fenton process.

The effect of temperature on removal ratio of MO was investigated. As shown in Fig. 3(c), temperature had no significant effect on removal ratio of MO in the photo-Fenton process catalyzed by $H_3PMo_{12}O_{40}$/organobentonite. However, the removal ratio of MO reached a high valve ($\eta(\%) \geqslant 87.9\%$) in temperature range from 30 to 70℃, which indicated that $H_3PMo_{12}O_{40}$/organobentonite had a wide applicable range of temperature for wastewater treatment. In any

(c)
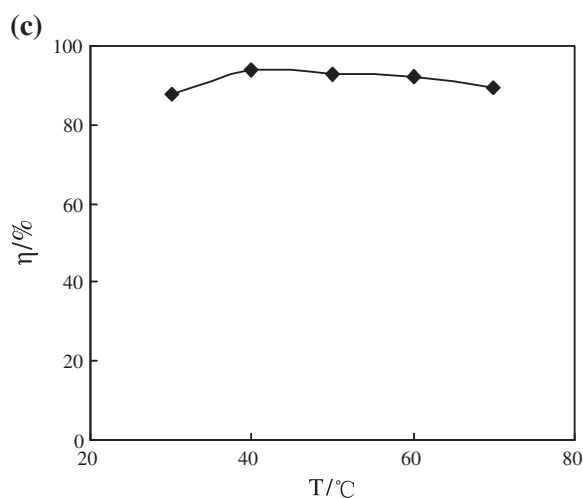
Fig. 3c. Effect of temperature on removal ratio of MO. The experimental conditions were conducted under conditions: $[MO] = 10 \, mg \, L^{-1}$, $[H_2O_2] = 8.8 \, mmol \, L^{-1}$, $t = 120 \, min$, $[H_3PMo_{12}O_{40}/organobentonite] = 1 \, g \, L^{-1}$, initial pH of solution.

(d)
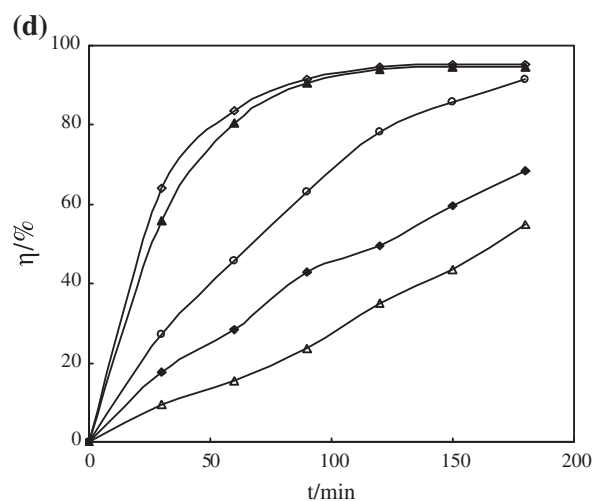
Fig. 3d. Effect of initial MO concentration ($\diamond$ $5 \, mg \, L^{-1}$, $\blacktriangle$ $10 \, mg \, L^{-1}$, $\circ$ $20 \, mg \, L^{-1}$, $\blacklozenge$ $30 \, mg \, L^{-1}$, $\triangle$ $40 \, mg \, L^{-1}$) on removal ratio. The experimental conditions were conducted under conditions: $[H_2O_2] = 8.8 \, mmol \, L^{-1}$, $[H_3PMo_{12}O_{40}/organobentonite] = 1 \, g \, L^{-1}$, initial pH of solution, $T = 40 \, ℃$.

case, temperature was a key parameter that had to be taken into account in photo-Fenton process, and usually it should be controlled at a specific value to obtain a high degradation of organic pollutant and effective use of H_2O_2. Controlling and holding temperature at specific value might cause some disadvantages for photo-Fenton process in practical applications. The wide applicable temperature range of $H_3PMo_{12}O_{40}$/organobentonite in photo-Fenton process improved the application performance of photo-Fenton process.

The effect of initial MO concentration on the removal ratio of MO was investigated, and the results were shown in Fig. 3(d). The removal ratio of MO with initial concentration of 5~10 mg/L increased quickly with the reaction time, and the removal ratio exceeded 90% in 120 min. By contrast, the removal ratio of MO with initial concentration of 20~50 mg/L increased slowly with the reaction time, especially for the MO wastewater with initial concentration over 20 mg/L. The decrease in removal ratio with an increase in MO concentration can be attributed to the greater amount of dye competing for degradation and/or the reduction in the light intensity that reaches the $H_3PMo_{12}O_{40}$/organobentonite surface.

Analysis of heterogeneous catalytic kinetics to degradation date has relied largely on well-known Langmuir-Hinshelwood (L-H) rate forms, which assume equilibrated adsorption of reactants and, correspondingly, a slow, rate-controlling surface step. Several researchers have reported that heterogeneous-catalyzed oxidative

Table 2
Kinetic models and regression coefficients

$C_0/(mg/L)$	Pseudo-first-order rate model			Pseudo-zero-order rate model		
	Eq.	$k/(min^{-1})$	R^2	Eq.	$k/(mg/(L\,min))$	R^2
5	$-\ln(1-x) = 0.0264t$	0.0264 ± 0.0013	0.9690	—	—	—
10	$-\ln(1-x) = 0.0249t$	0.0249 ± 0.0008	0.9877	—	—	—
20	$-\ln(1-x) = 0.0129t$	0.0129 ± 0.0004	0.9832	$x = 0.0059t$	0.0059 ± 0.0003	0.9152
30	—	—	—	$x = 0.0041t$	0.0041 ± 0.0001	0.9688
40	—	—	—	$x = 0.0029t$	0.0029 ± 0.0001	0.9925

degradation of organic dyes at low concentrations often follows L-H kinetics [26,27]. The L-H rate formulations can be transformed into pseudo-first-order rate model (Eq. (4)) and pseudo-zero-order rate model (Eq. (5)) at low concentration and high concentration, respectively.

$$-\ln(1 - x) = kt \tag{4}$$

$$x = kt \tag{5}$$

where x denotes the fraction of the MO degradation, k denotes the rate constant, and t denotes the reaction time. The rate constants and their regression coefficients for photo-Fenton degradation of MO using $H_3PMo_{12}O_{40}$/organobentonite catalyst had been calculated with pseudo-first-order rate model (Eq. (4)) and pseudo-zero-order rate model (Eq. (5)), and the results of kinetic models were presented in Table 2. It was seen that the photo-Fenton degradation of MO catalyzed with $H_3PMo_{12}O_{40}$/organobentonite followed the pseudo-first-order rate model at $C_0 \leqslant 20\,mg/L$, and the photo-Fenton degradation of MO followed the pseudo-zero-order rate model at $C_0 \geqslant 20\,mg/L$. The correlation coefficient indicated a good fit for all the obtained parameters ($R^2 > 0.9$).

In order to study the long-term stability of $H_3PMo_{12}O_{40}$/organobentonite used in photo-Fenton process, the stability of catalyst was tested with used $H_3PMo_{12}O_{40}$/organobentonite. The variation between the removal ratio and the recycling times of used catalyst was shown in Fig. 3(e). The results showed that $H_3PMo_{12}O_{40}$/organobentonite retained most of its catalytic stability and activity for four recycling times, which indicated that $H_3PMo_{12}O_{40}$ chemically immobilized in the interlayer space of organobentonite had not leached from catalyst. It was interesting to note that the removal ratio had slightly increased after the first use of catalyst, which could be caused by the degradation of CTAB alkylchains during the first use of catalyst. $H_3PMo_{12}O_{40}$/organobentonite had an excellent long-term stability in the photo-Fenton
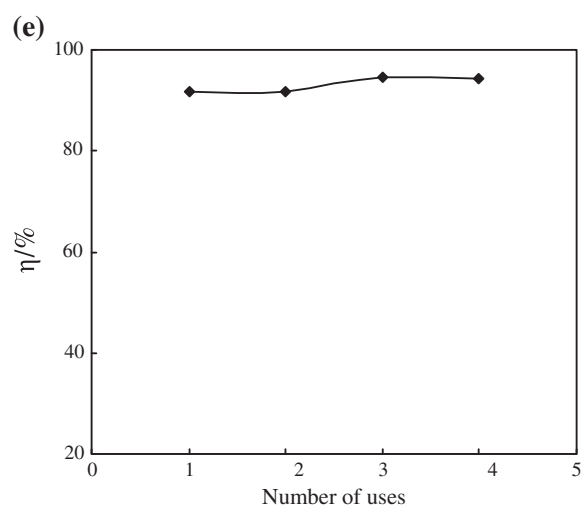
Fig. 3e. Variation between the removal ratio of MO and the number of catalyst use. The experimental conditions were conducted under conditions: $[MO] = 10\,mg\,L^{-1}$, $[H_3PMo_{12}O_{40}/$organobentonite$] = 1\,g\,L^{-1}$, $[H_2O_2] = 8.8\,mmol\,L^{-1}$, $t = 120\,min$, initial pH of solution, $T = 40°C$.

process. Moreover, compared to the catalyst of metal ions in homogeneous photo-Fenton process, $H_3PMo_{12}O_{40}$/organobentonite as heterogeneous catalyst can easily been separated from the treated wastewater system, and been reused in the next photo-Fenton process of wastewater treatment.

3.4. Catalyst characterization, preparation mechanism, and its reaction mechanism in photo-Fenton

The XRD pattern of the $H_3PMo_{12}O_{40}$/organobentonite (Fig. 4(a)) showed a reflection peak at about 2θ 6.125°, corresponding to a interlayer spacing of 1.4418 nm which indicated that $H_3PMo_{12}O_{40}$ (about 1 nm in diameter [28]) could be chemically and molecularly immobilized in the interlayer space of organobentonite. Moreover, little reflections emerged at 2θ 10.673°, 15.224°, 18.650°, 28.417°, 30.718°, and 31.382° in the XRD patterns. Matching the XRD pattern with reference patterns of pure substances (e.g. ammonium

(a)

(b)

(c)
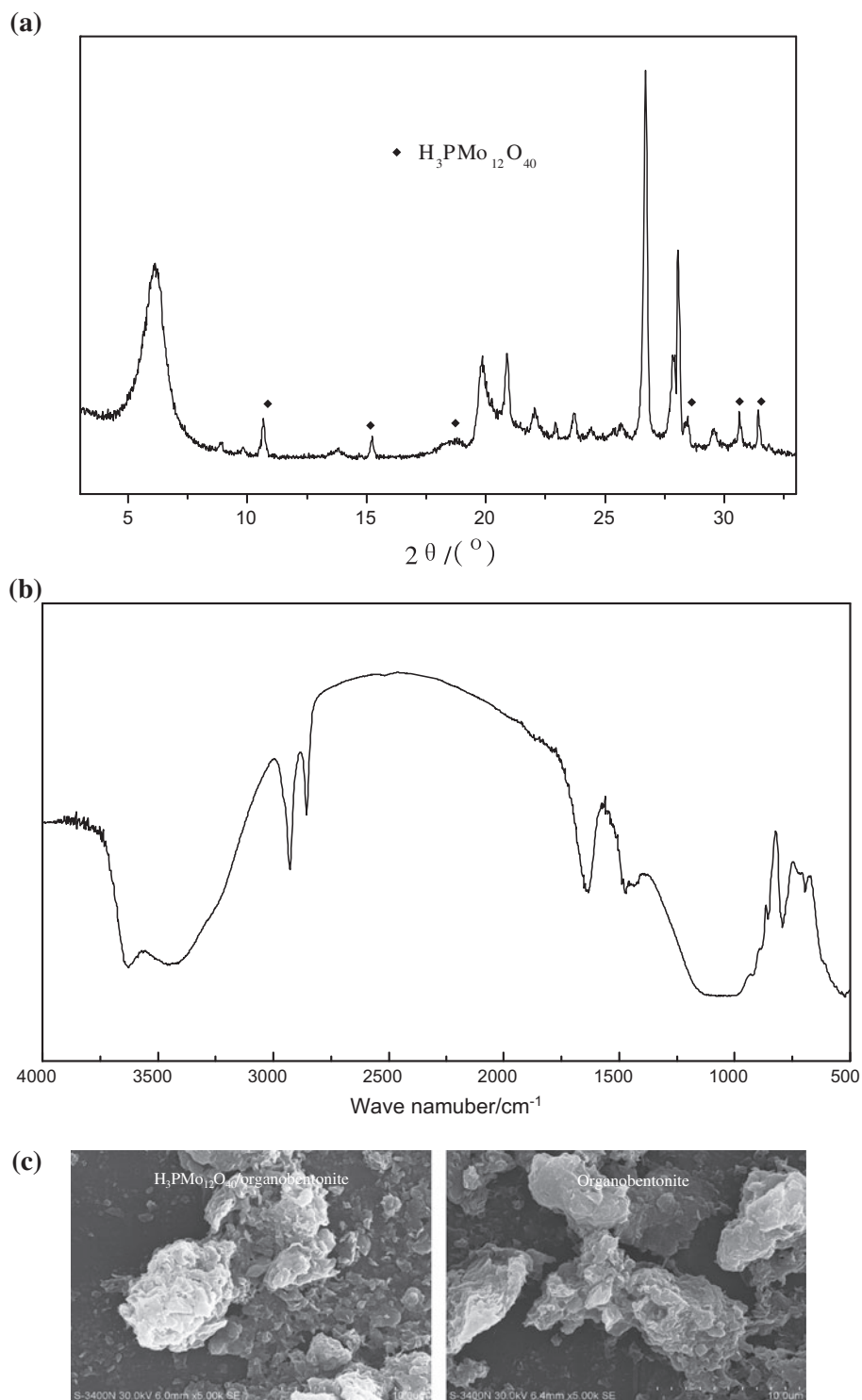
Fig. 4. (a) XRD patterns of $H_3PMo_{12}O_{40}$/organobentonite, (b) FT-IR spectra of $H_3PMo_{12}O_{40}$/organobentonite and (c) SEM pictures of $H_3PMo_{12}O_{40}$/organobentonite and organobentonite.

molybdenum oxide phosphate hydrate, PDF#16–0, 181), the little reflections mentioned above might be attributed to the crystalline phase of ammonium phosphomolybdate hydrate.
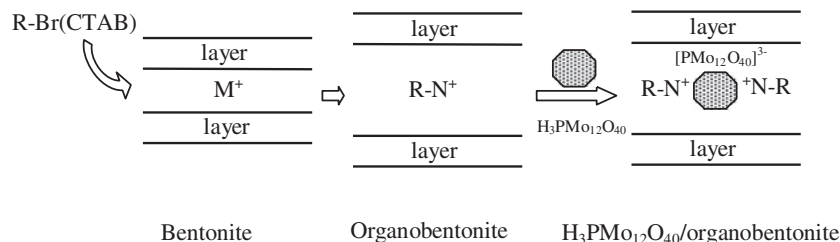
Fig. 5. Schematic procedures for $H_3PMo_{12}O_{40}$/organobentonite.

FT-IR spectra (4,000–500 cm^{-1}) of catalyst were presented in Fig. 4(b). Sharp absorption bands of CTAB at approximately 2,937, 2,854, and 1,470 cm^{-1} were observed. The first two bands could be assigned to the symmetric and asymmetric stretching vibrations of methyl and methylene groups, while the third one corresponded to their bending vibrations [29]. Moreover, two peaks emerged at 854 and 792 cm^{-1}. The former was the interoctahedral Mo–O–Mo band of keggin $H_3PMo_{12}O_{40}$ which immobilized on organobentonite; the latter was the intraoctahedral Mo–O–Mo band of keggin $H_3PMo_{12}O_{40}$ [30,31]. It was found that the characteristic IR bands of $H_3PMo_{12}O_{40}$ in the $H_3PMo_{12}O_{40}$/organobentonite appeared at shifted positions compared to those of unsupported $H_3PMo_{12}O_{40}$, indicating a strong chemical interaction between $H_3PMo_{12}O_{40}$ and organobentonite. P–O bending vibration (1,064 cm^{-1}) and W=O bending vibration (964 cm^{-1}) disappeared in the spectrum of $H_3PMo_{12}O_{40}$/organobentonite, which was attributable to overlapping with the characteristic peak of bentonite at around 1,000 cm^{-1} [32].

Fig. 4(c) showed SEM pictures of $H_3PMo_{12}O_{40}$/organobentonite and organobentonite. Compared with organobentonite, $H_3PMo_{12}O_{40}$/organobentonite was a material with smaller fragments and clearer sheet structure. The SEM differences between $H_3PMo_{12}O_{40}$/organobentonite and organobentonite showed that $H_3PMo_{12}O_{40}$ was successfully immobilized on organobentonite.

Based on the characterization of $H_3PMo_{12}O_{40}$/organobentonite, the schematic procedures for the organobentonite and the subsequent immobilization of $H_3PMo_{12}O_{40}$ on the organobentonite were presented in Fig. 5. When bentonite is in contact with other ions in aqueous dispersion, the interlayer cations in the crystals of montmorillonite can be exchanged by the cations in aqueous dispersion, namely ion-exchange performance of bentonite. Because of the ion-exchange performance of bentonite, CTAB exchanged with the interlayer cations, and then intercalated into interlayer space of montmorillonite crystal, which was the mechanism of organobentonite formation. The

intercalation of CTAB was cation exchange reaction as Eq. (6).

$$R\text{-}Br(CTAB) + M\text{-}bentonite \rightarrow R\text{-}bentonite + M^+ + Br^- \tag{6}$$
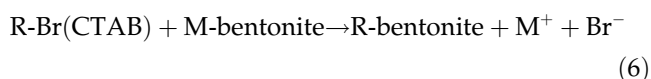
where R was alkylchains of CTAB. The quaternary ammonium groups in the interlayer space of montmorillonite crystal were anchoring sites for $H_3PMo_{12}O_{40}$, and then $H_3PMo_{12}O_{40}$ could be chemically and molecularly immobilized in the interlayer space of montmorillonite crystal in organobentonite, and $H_3PMo_{12}O_{40}$/organobentonite was obtained.

HPA effectively stimulating the generation of hydroxyl radicals from H_2O_2 in the UV–H_2O_2 process had been reported [10,19]. Based on the present results and our previous study [19], the possible mechanisms of photo-Fenton process were proposed as follows: the HPA salt formed on organobentonite ($\vdash$ HPS) could be photo-oxidized into $\vdash$ HPS* under the action of UV light, as shown in Eq. (7). reacted with H_2O_2 and H_2O to generate hydroxyl radicals, and $\vdash$ HPS* was transformed into $\vdash$ HPS$^-$ which was in reducing state as shown in Eqs. (8) and (9). $\vdash$ HPS$^-$ could be reduced into $\vdash$ HPS by O_2 as shown in Eq. (10). Hydroxyl radicals, which is highly oxidative, could attack the MO adsorbed on the surface of $H_3PMo_{12}O_{40}$/organobentonite and MO was finally degraded into CO_2 and H_2O (Eq. (11)).

$$\vdash HPS \xrightarrow{h\nu} \vdash HPS^* \tag{7}$$

$$2 \vdash HPS^* + H_2O_2 \rightarrow 2 \vdash HPS + 2 \cdot OH \tag{8}$$

$$\vdash HPS^* + H_2O \rightarrow \vdash HPS + \cdot OH + H^+ \tag{9}$$

$$\vdash HPS + O_2 \rightarrow \vdash HPS + O_2 \tag{10}$$

$$MO + OH \rightarrow Degradations\ (CO_2 + H_2O) \tag{11}$$
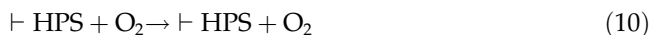
4. Conclusions

$H_3PMo_{12}O_{40}$ was chemically immobilized on the organobentonite through grafting, and $H_3PMo_{12}O_{40}/$ organobentonite was prepared. $H_3PMo_{12}O_{40}/$organobentonite had been applied to photo-Fenton degradation of MO to study its catalytic performance as heterogeneous catalyst in photo-Fenton process. The results showed that the removal ratio of MO was impacted by reaction time, H_2O_2 concentration, and initial MO concentration. $H_3PMo_{12}O_{40}/$organobentonite had a wide applicable range of pH and temperature for wastewater treatment. Moreover, $H_3PMo_{12}O_{40}/$organobentonite had a long-term stability, and retained almost all of its catalytic stability and activity for four recycling times. $H_3PMo_{12}O_{40}/$organobentonite had certain advantages for practical use in photo-Fenton process. Characterization results of $H_3PMo_{12}O_{40}/$organobentonite showed that the $H_3PMo_{12}O_{40}$ was immobilized on the catalyst. The possible mechanisms involving in both catalyst preparation and photo-Fenton process were presented in paper.

References

[1] S. Trabelsi-Souissi, N. Oturan, N. Bellakhal, M.A. Oturan, Application of the photo-Fenton process to the mineralization of phthalic anhydride in aqueous medium, Desalin. Water Treat. 25 (2011) 210–215.

[2] D. Melgoza, A. Hernández-Ramírez, J.M. Peralta-Hernández, Comparative efficiencies of the decolourisation of Methylene Blue using Fenton's and photo-Fenton's reactions, Photochem. Photobiol. Sci. 8 (2009) 596–599.

[3] J. Feng, X. Hu, P.L. Yue, Discoloration and mineralization of Orange II using different heterogeneous catalysts containing Fe: A comparative study, Environ. Sci. Technol. 38 (2004) 5773–5778.

[4] J.H. Ramirez, M.A. Vicente, L.M. Madeira, Heterogeneous photo-Fenton oxidation with pillared clay-based catalysts for wastewater treatment: A review, Appl. Catal. B: Environ. 98 (2010) 10–26.

[5] G.T. Wei, C.Y. Fan, L.Y. Zhang, R.C. Ye, T.Y. Wei, Z.F. Tong, Photo-Fenton degradation of methyl orange using $H_3PW_{12}O_{40}$ supported Fe-bentonite catalyst, Catal. Commun. 17 (2012) 184–188.

[6] T. Okuhara, N. Mizuno, M. Misono, Catalytic chemistry of heteropoly compounds, Adv. Catal. 41 (1996) 113–225.

[7] M.Q. Hu, Y.M. Xu, Photocatalytic degradation of textile dye X3B by heteropolyoxometalate acids, Chemosphere 54 (2004) 431–434.

[8] L. Wang, Photocatalytic degradation of methyl orange solution with phosphotungstic acid, Environ. Sci. Technol. (In Chinese) 29 (2006) 35–39.

[9] Y. Kamiya, T. Okuhara, M. Misono, A. Miyaji, K. Tsuji, T. Nakajo, Catalytic chemistry of supported heteropolyacids and their applications as solid acids to industrial processes, Catal. Surv. Asia. 12 (2008) 101–113.

[10] S.T. Li, M. Gao, Y. Tao, Study on degradation of Crystal Violet by UV/Fenton/Heteropolyacid system, in: Proceedings of the Third International Conference on Bioinformatics and Biomedical Engineering, Beijing, 2009, pp. 1–4.

[11] H. Kim, J.C. Jung, S.H. Yeom, K.Y. Lee, J. Yi, I.K. Song, Immobilization of a heteropolyacid catalyst on the aminopropyl-functionalized mesostructured cellular foam (MCF) silica, Mater. Res. Bull. 42 (2007) 2132–2142.

[12] L.C. Passoni, F.J. Luna, M. Wallau, R. Buffon, U. Schuchardt, Heterogenization of $H_6PMo_9V_3O_{40}$ and palladium acetate in VPI-5 and MCM-41 and their use in the catalytic oxidation of benzene to phenol, J. Mol. Catal. A: Chem. 134 (1998) 229–235.

[13] K. Nowińska, W. Kaleta, Synthesis of Bisphenol-A over heteropoly compoundsencapsulated into mesoporous molecular sieves, Appl. Catal. A: Gen. 203 (2000) 91–100.

[14] W. Kaleta, K. Nowinska, Immobilisation of heteropoly anions in Si-MCM-41 channels by means of chemical bonding to aminosilane groups, Chem. Commun. 6 (2001) 535–536.

[15] L.X. Zhang, Q.Z. Jin, L. Shan, Y.F. Liu, X.G. Wang, J.H. Huang, $H_3PW_{12}O_{40}$ immobilized on silylated palygorskite and catalytic activity in esterification reactions, Appl. Clay Sci. 47 (2010) 229–234.

[16] A.C. Yip, F.L. Lam, X. Hu, Chemical vapor deposited copper on acid-activated bentonite clay as an applicable heterogeneous catalyst for the photo-Fenton-like oxidation of textile organic pollutants, Ind. Eng. Chem. Res. 44 (2005) 7983–7990.

[17] E.G. Ramírez, B.G. Theng, M.L. Mora, Clays and oxide minerals as catalysts and nanocatalysts in Fenton-like reactions—A review, Appl. Clay Sci. 47 (2010) 182–192.

[18] A.N. Soon, B.H. Hameed, Heterogeneous catalytic treatment of synthetic dyes in aqueous media using Fenton and photo-assisted Fenton process, Desalination 269 (2011) 1–16.

[19] G.T. Wei, L.Y. Zhang, T.Y. Wei, Q.Y. Luo, Z.F. Tong, UV-H_2O_2 degradation of methyl orange catalysed by $H_3PW_{12}O_{40}/$activated clay, Environ. Technol. 33 (2012) 1589–1595.

[20] G.T. Wei, Z.M. Li, D.K. Liao, Z.F. Tong, Adsorption and decolouration process of molasses alcohol wastewater (in Chinese), J. Chem. Eng. Chin. Uni. 18 (2004) 414–419.

[21] G.T. Wei, Z.F. Tong, D.K. Liao, Z.M. Li, X.L. Bao, Y.X. Jiang, Adsorption behaviour of molasses alcohol wastewater on organobentonite, in: Proceedings of the Fourth International Conference on Separation Science and Technology, Nanning, 2004, pp. 517–522.

[22] J. Fernandez, J. Bandara, A. Lopez, P. Buffar, J. Kiwi, Photo-assisted Fenton degradation of nonbiodegradable azo dye (Orange II) in Fe-free solutions mediated by cation transfer membranes, Langmuir 15 (1999) 185–192.

[23] A.A. Fatema, S.A. Amna, M.A. Maitha, A.R. Muhammad, A. Salman, Comparative efficiencies of the degradation of Crystal Violet using UV/hydrogen peroxide and Fenton's reagent, Dyes Pigm. 74 (2007) 283–287.

[24] M. Tokumura, A. Ohta, H.T. Znad, Y. Kawase, UV light assisted decolorization of dark brown colored coffee effluent by photo-Fenton reaction, Water Res. 40 (2006) 3775–3784.

[25] Y.S. Jung, W.T. Lim, J.Y. Park, Y.H. Kim, Effect of pH on Fenton and Fenton-like oxidation, Environ. Technol. 30 (2009) 183–190.

[26] F. Emami, A.R. Tehrani-Bagha, K. Gharanjig, F.M. Menger, Kinetic study of the factors controlling Fenton-promoted destruction of a non-biodegradable dye, Desalination 257 (2010) 124–128.

[27] Y.R. Smith, A. Kar, V. Subramanian, Investigation of physico-chemical parameters that influence photocatalytic degradation of methyl orange over TiO_2 nanotubes, Ind. Eng. Chem. Res. 48 (2009) 10268–10276.

[28] T. Kurucsev, A.M. Sargeson, B.O. West, Size and hydration of inorganic ions from viscosity and density measurements, J. Phys. Chem. 61 (1957) 1567–1569.

[29] A.S. Özcan, B. Erdem, A. Özcan, Adsorption of Acid Blue 193 from aqueous solutions onto Na-bentonite and DTMA-bentonite, J. Colloid Interf Sci. 280 (2004) 44–54.

[30] H. Kim, J.C. Jung, P. Kim, S.H. Yeom, K.Y. Lee, I.K. Song, Preparation of $H_3PMo_{12}O_{40}$ catalyst immobilized on surface modified mesostructured cellular foam (SM-MCF) silica and its application to the ethanol conversion reaction, J. Mol. Catal. A: Chem. 259 (2006) 150–155.

[31] H. Kim, P. Kim, K.Y. Lee, S.H. Yeom, J. Yi, I.K. Song, Preparation and characterization of heteropolyacid/mesoporous carbon catalyst for the vapor-phase 2-propanol conversion reaction, Catal. Today 111 (2006) 361–365.

[32] C. Paluszkiewicz, M. Holtzer, A. Bobrowski, FTIR analysis of bentonite in moulding sands, J. Mol. Struct. 880 (2008) 109–114.